



Optimization of the Acoustic Performance of a Composite Multi-cell Sound Absorber

Jiangmei Liang¹ · Zhengqing Liu^{1,2,3} · Qiucheng Wang¹ · Yujun Zhao⁴ · Mohammad Fard⁴ · John Laurence Davy⁵

Received: 21 February 2023 / Accepted: 27 April 2023 / Published online: 17 May 2023
© Australian Acoustical Society 2023

Abstract

The sound absorption coefficient (SAC) of a composite multi-cell sound absorber in the low- and mid-frequency range is investigated by using experiment and numerical method. The composite sound absorber includes a MPP (micro-perforated panel) layer, a porous material layer, and an air cavity layer. The sandwich acoustic structure consists of an air cavity layer in between two MPP layers, which is backed by another air cavity layer. Maa's model was used to describe the MPP layer, and the porous material layer was established by using Delany and Bazley's model. The transfer matrix method (TMM) was used to calculate the surface impedance of each acoustic unit-cell of the composite multi-cell sound absorber, and the SAC of the composite multi-cell sound absorber was predicted by using the equivalent circuit method. Finite element (FE) models of the composite multi-cell sound absorbers are presented, and their sound absorption coefficient was measured by using an impedance tube method. The measurement data demonstrate the validity of the prediction results and are used to analyse various acoustic characteristics that depend on the structural parameters of each acoustic unit-cell. Furthermore, an optimal combination of the structural parameters of the composite multi-cell sound absorber can be realized by using the genetic algorithm (GA). The effect of the number of the acoustic unit-cells with different perforation ratios of the MPP layer and the depth of the air cavity layer is presented. They are the main design parameters that can control the SAC in different frequency ranges. The results also show that the SAC of the composite multi-cell sound absorber can be adjusted by increasing the number of the acoustic unit-cells and using the optimized design of the air cavity layer.

Keywords Composite multi-cell sound absorber · Sound absorption coefficient · Genetic algorithm · Transfer matrix method · Impedance tube method

1 Introduction

Acoustic materials and sound-absorbing structures have been widely used in different engineering areas, such as

architecture, ships, vehicles, railways and aerospace [1–6]. The familiar acoustic structures and materials are usually a micro-perforated panel (MPP) [7, 8] and porous sound-absorbing material [9, 10]. They can reduce the sound standing waves to enhance the acoustic quality of an enclosure interior system and do not need external energy input. However, the frequently used microperforated panels have poor sound absorption properties in the low- and mid-frequency range with a narrow sound absorption bandwidth [11]. In recent years, sound absorption in the low- and mid-frequency range has been investigated by different methods including mechanical impedance plates [12], super-aligned carbon nanotube arrays [13], MPPs with arbitrary cross-sectional perforations [14], etc. Most studies have obtained broadband sound absorption by using multilayer arrangements and parallel layouts, where the combination of resistive and reactive acoustic materials can

✉ Zhengqing Liu
liuzhengqing@zjut.edu.cn

¹ College of Mechanical Engineering, Zhejiang University of Technology, Hangzhou 310023, China
² Henan Provincial Engineering Laboratory of Automotive Composite Materials, Henan University of Technology, Zhengzhou 450001, China
³ Zhejiang Jiuzhou New Energy Technology Co., Ltd, Taizhou 317523, China
⁴ School of Engineering, RMIT University, Bundoora 3083, Australia
⁵ School of Science, RMIT University, Melbourne 3001, Australia

effectively improve the SAC and broaden the sound absorption band.

In the early research, Maa [15] presented an acoustic structure consisting of two MPP layers with different structural parameters. The acoustic performance was improved at low and mid frequencies. In their research, Zhang and Gu [16] and Sakagami et al. [17] extended the acoustic structure designed by Maa and increased the sound absorption coefficient to some extent. Kim et al. [18, 19] proposed multi-layered MPPs and considered the fluid—solid coupling between the MPPs and the air gaps. The acoustic performance of multi-layered infinite MPPs and multi-layered elastic MPPs was presented and discussed. Park [20] designed an MPP structure backed by Helmholtz resonators with different necks, utilizing the low-frequency SAC of the resonators to realize broadband absorption performance. Wang et al. [21] numerically and experimentally investigated an MPP structure backed by an irregular-shaped air cavity, and the results showed that the altered vibro-acoustic coupling pattern of the irregular arrangement could significantly improve the SAC of the acoustic structure. In their research, Liu et al. [22] investigated a multilayer sound absorber. The results showed that the use of a porous material behind the MPP and backed by an air cavity could broaden the sound absorption frequency band. Yilmazer et al. [23] studied the sound absorption performance of a porous expanded perlite. The results showed that the water content and fibre mixture had a certain influence on the sound absorption performance. Sakagami et al. [24] proposed a type of sound absorber, which has a double MPP arrangement with different perforation rates and different depths of the air layer. Gai et al. [25] studied a two-MPP parallel arrangement backed by an L-shaped air cavity structure whose depth was computed from the inlet area and the total volume. Kim et al. [26] designed a parallel-arranged MPP, and the influences of rigid partitions were presented using the finite element method with the plane wave conditions. Li et al. [27] presented a parallel-arranged MPP absorber that consisted of four perforated panels that could obtain more than one octave of sound absorption bandwidth in the low-frequency range. A case study of an MPP with heterogeneous hole sizes and perforation ratios was presented by Midori et al. [28]. In their research, the sound absorption coefficient of the acoustic structure was measured using the impedance tube method and validated using a theoretical model. Zhao et al. [29] designed a double-porosity material composed of porous sound-absorbing material and a labyrinthine channel. The theoretical, the numerical and the experimental results showed that the double-porosity material had good sound absorption performance in low frequencies. Faisal et al. [30] proposed a single layer of four

parallel-arranged microperforated panels absorber by optimization of hole diameter, perforation ratio and cavity depths. However, their results show that only absorption bandwidth below 500 Hz is improved. In this study, composite multi-cell sound absorbers consisting of different acoustic unit-cells containing an MPP layer, a porous material layer, and an air cavity layer were designed. The proposed composite sound absorber can increase the peak SAC and produce a wider sound absorption bandwidth in the low- and mid-frequency range if the structural parameters of each acoustic unit-cell are optimized.

This paper has been organized as follows: The theoretical method is presented in Sect. 2 and is used to calculate the SAC of the composite multi-cell sound absorber. In Sect. 3, the two-microphone impedance tube method is used to measure the SAC of the proposed composite multi-cell sound absorber. The finite element model of the impedance tube is presented in Sect. 4. In Sect. 5, the experiment data and the prediction results are compared and discussed. Moreover, the influences of the constitutive parameters of the composite multi-cell sound absorber are investigated. This includes the effect of the number of the acoustic unit-cells, the perforation ratio, and the depth of the air cavity layer. In addition, GA was used to optimize the composite multi-cell sound absorbers to obtain the maximum sound absorption performance. Finally, the conclusions are presented in Sect. 6.

2 Theoretical Formulations

Figure 1 shows the schematic diagram of the composite multi-cell sound absorber with different acoustic unit-cells. The composite sound absorber included an MPP sound absorber, a porous material, and an air cavity layer in that order. The sandwich acoustic structure consisted of an air cavity in between two MPP layers backed by another air cavity layer. It should be noted that the MPP layer of each acoustic unit-cell of the sound absorber has a different perforation ratio and is backed by either equal or unequal air cavities. In addition, each acoustic unit-cell is separated by a rigid wall. In this study, Maa's model [15] and Delany-Bazley's model [31] were used to describe the MPP layer and the porous material layer, respectively. The analytical model was constructed by utilizing the TMM [32, 33] to calculate the surface impedance of each acoustic unit-cell, and the SAC of the composite multi-cell sound absorber was calculated by using the equivalent circuit method [34, 35].

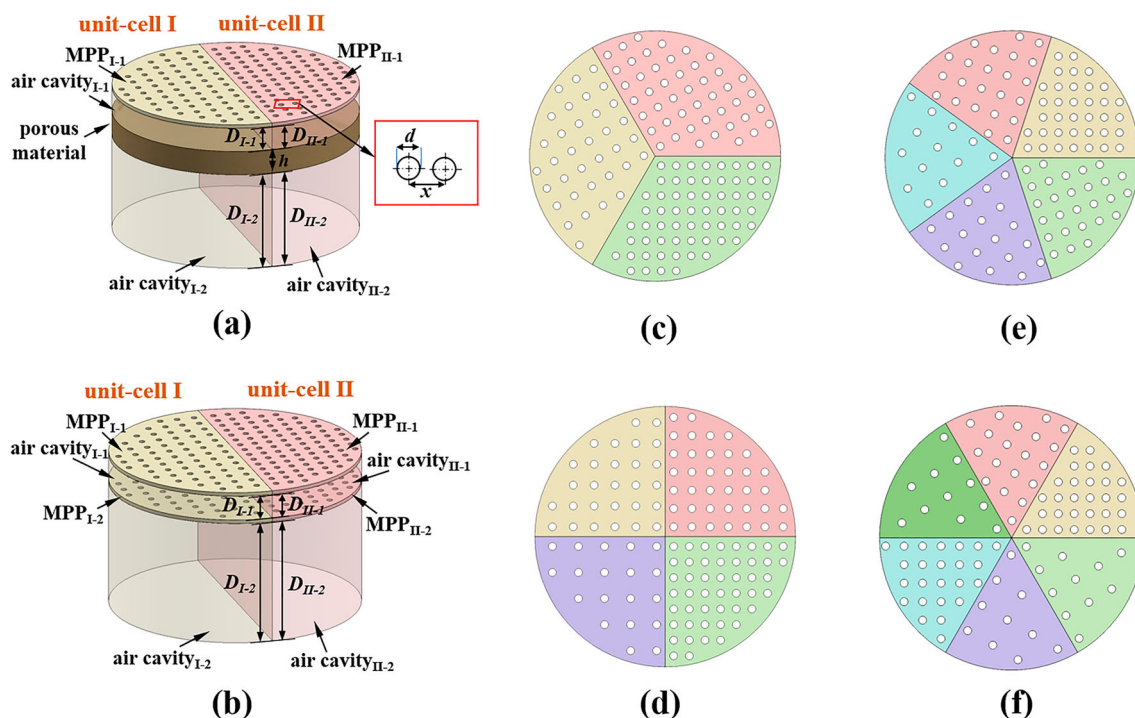


Fig. 1 Schematic diagram of **a** the composite sound absorber with two acoustic unit-cells, **b** the sandwich acoustic structure with two acoustic unit-cells, and the perforated panels for **c** three acoustic unit-cells, **d** four acoustic unit-cells, **e** five acoustic unit-cells, and **f** six acoustic unit-cells

2.1 Acoustic Impedance of the Composite Multi-cell Sound Absorber

2.1.1 Micro-Perforated Plate (MPP) Layer

In this paper, the calculation of acoustic impedance Z_{MPP} of the MPP layer is based on Maa’s theory [36, 37], which is described by the following equation:

$$Z_{MPP} = \rho_0 c_0 (r + j\omega m) \tag{1}$$

where ρ_0 is the ambient air density, c_0 is the speed of the sound in air, $\omega = 2\pi f$ is the angular frequency related to frequency f , r and m are the relative acoustic resistance and relative acoustic reactance of the MPP layer, respectively, and they can be calculated by:

$$r = \frac{32\eta t}{pd^2} \left(\sqrt{1 + \frac{k^2}{32}} + \frac{\sqrt{2} kd}{t} \right) \tag{2}$$

$$m = \frac{t\rho_0}{p} \left(1 + \frac{1}{\sqrt{9 + \frac{k^2}{2}}} + \frac{0.85d}{t} \right) \tag{3}$$

where η is the kinematic viscosity coefficient of the ambient air, t is the thickness of the MPP layer, p and d are the perforation ratio and the hole diameter of the MPP layer,

respectively. The hole spacing x can be calculated by $x = (p/4\pi d^2)^{-2}$, and the perforate constant k can be calculated by:

$$k = \frac{d}{2} \sqrt{\omega\rho_0/\eta} \tag{4}$$

and the transfer matrix T_{MPP} of the MPP layer can be written as:

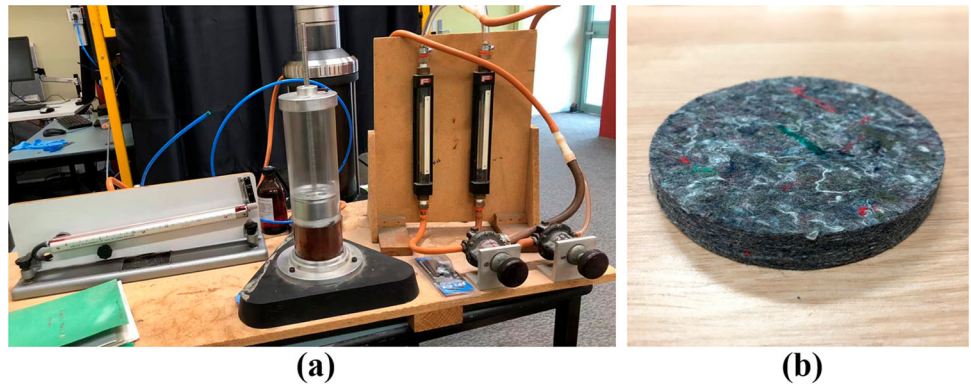
$$T_{MPP} = \begin{bmatrix} 1 & Z_{MPP} \\ 0 & 1 \end{bmatrix} \tag{5}$$

2.1.2 Porous Material Layer

In this study, the characteristic impedance Z_c and the complex wavenumber k_c of the porous sound-absorbing material layer are calculated by using Delany and Bazley’s model [31], which is quite effective for the prediction of the sound absorption coefficient for a porous fibrous material. They can be calculated by using the following expressions:

$$Z_c = \rho_0 c_0 \left[1 + 0.0571 \left(\frac{\rho_0 f}{\sigma} \right)^{-0.754} - j0.087 \left(\frac{\rho_0 f}{\sigma} \right)^{-0.732} \right] \tag{6}$$

Fig. 2 Measurement of the airflow resistivity of the porous fibrous material: **a** the experimental setup of the air flow resistivity apparatus and **b** the porous fibrous material test sample



$$k_c = \frac{\omega}{c_0} \left[1 + 0.0978 \left(\frac{\rho_0 f}{\sigma} \right)^{-0.700} - j 0.189 \left(\frac{\rho_0 f}{\sigma} \right)^{-0.595} \right] \tag{7}$$

In this model, the air flow resistivity σ is an important parameter that needs to be obtained by measurement. As shown in Fig. 2a, the air flow resistivity of the selected porous fibrous material was measured by using an air flow resistivity measuring instrument according to the ASTM C522-03 standard [38]. In this paper, the average thickness and the measured airflow resistivity of the selected porous fibrous material test sample (as shown in Fig. 2b) are $h = 10$ mm and $\sigma = 92,033$ N s/m⁴, respectively.

The transfer matrix T_{porous} of the porous sound-absorbing material layer can be written as:

$$T_{\text{porous}} = \begin{bmatrix} \cos(k_c h) & j Z_c \sin(k_c h) \\ j \sin(k_c h) / Z_c & \cos(k_c h) \end{bmatrix} \tag{8}$$

where h is the thickness of the porous material layer.

2.1.3 Air Cavity Layer

The rigidly backed air cavity layer is significant for sound absorption. The characteristic impedance Z_0 and the wave number k_0 of the air in an air cavity with a depth of D can be calculated by using the following expressions:

$$Z_0 = \rho_0 c_0 \tag{9}$$

$$k_0 = \frac{\omega}{c_0} \tag{10}$$

and the transfer matrix T_{air} of the air cavity layer can be written as:

$$T_{\text{air}} = \begin{bmatrix} \cos(k_0 D) & j Z_0 \sin(k_0 D) \\ j \sin(k_0 D) / Z_0 & \cos(k_0 D) \end{bmatrix} \tag{11}$$

2.2 Sound Absorption Coefficient of the Composite Multi-Cell Sound Absorber

The total transfer matrix T_{total} of each acoustic unit-cell of the composite sound absorber (as shown in Fig. 1a) can be calculated by connecting the individual transfer matrices of each layer in order [32, 33]:

$$T_{\text{total}} = T_{\text{MPP}_{i-1}} \cdot T_{\text{air}_{i-1}} \cdot T_{\text{porous}} \cdot T_{\text{air}_{i-2}} = \begin{bmatrix} T_{11} & T_{12} \\ T_{21} & T_{22} \end{bmatrix} \tag{12}$$

Similarly, the total transfer matrix T_{total} of each acoustic unit-cell of the sandwich acoustic structure, as shown in Fig. 1b, can be calculated by:

$$T_{\text{total}} = T_{\text{MPP}_{i-1}} \cdot T_{\text{air}_{i-1}} \cdot T_{\text{MPP}_{i-2}} \cdot T_{\text{air}_{i-2}} = \begin{bmatrix} T_{11} & T_{12} \\ T_{21} & T_{22} \end{bmatrix} \tag{13}$$

where $i = I, II, III \dots$ denote the different acoustic unit-cells for the composite multi-cell sound absorber. The surface impedance of each acoustic unit-cell of the composite multi-cell sound absorber can be obtained as follows:

$$Z_s = T_{11} / T_{21} \tag{14}$$

It is assumed that the MPP is so rigid that the vibration effect of the panel under acoustic loading can be neglected. The acoustic-electric analogy approach is employed to derive the total acoustic impedance Z_{total} of the composite multi-cell sound absorber with rigid partitions between the unit-cells, and the equivalent circuit of the composite multi-cell sound absorber is shown in Fig. 3. It is worth noting that in this circuit every acoustic impedance should be divided by the area ratio ε in advance, which is the ratio of the surface area of each acoustic unit-cell to the overall surface area [25, 28]. The surface impedance of the total composite multi-cell sound absorber can be obtained as follows [28]:

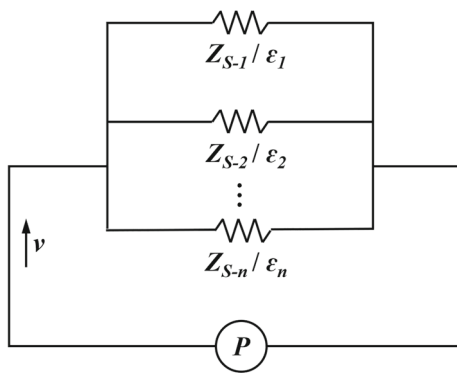


Fig. 3 The equivalent circuit of the composite multi-cell sound absorber

$$Z_{\text{total}} = \left(\sum_{i=1}^n \frac{\varepsilon_i}{Z_{S-i}} \right)^{-1} \tag{15}$$

Finally, the normal incidence sound absorption coefficient α of a composite multi-cell sound absorber can be calculated by:

$$\alpha = \frac{4\text{Re}(Z_{\text{total}}/Z_0)}{[1 + \text{Re}(Z_{\text{total}}/Z_0)]^2 + [\text{Im}(Z_{\text{total}}/Z_0)]^2} \tag{16}$$

3 Measurement

As shown in Fig. 4, the B&K impedance tube kit Type 4206 and the Pulse LabShop software were used to measure the SAC of the composite multi-cell sound absorber test specimens. The large tube was used and the SAC of the test specimens were measured in the frequency range from 50 to 1600 Hz. In this measurement, the two-microphone transfer function method was used according to the ASTM E1050-12 international standard [39]. It should be noted that the AM (Additive Manufacturing) method was used to fabricate a high-precision MPP test specimen with different structural parameters [22]. The designed thickness and the hole diameter of the MPP layer were $t = 1$ mm and $d = 0.6$ mm, respectively, and the designed structural parameters of the composite multi-cell sound absorbers with two acoustic unit-cells, three acoustic unit-cells and four acoustic unit-cells are listed in Tables 1, 2 and 3, respectively.

4 Numerical Model

An impedance tube FE model was used for numerical analysis of the sound absorption of the proposed composite multi-cell sound absorber. The FE model was established by using the COMSOL software for comparison with the SAC results obtained by experiment. As shown in Fig. 5, the pressure acoustic module was used to build the background

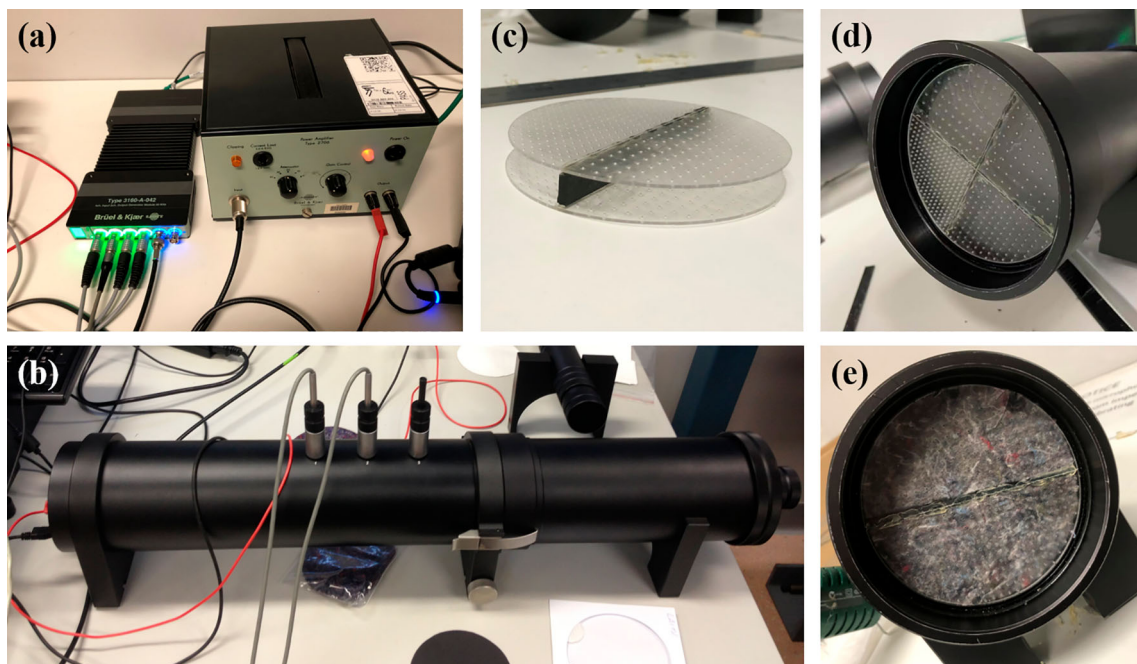


Fig. 4 Two-microphone impedance tube measurement system and the test specimens: **a** B&K Type 2706 power amplifier and B&K Type 3160-A-042 signal acquisition module, **b** B&K impedance tube kit Type 4206 and 1/4" pressure field microphone (Type 4187), **c** sandwich acoustic structure with two acoustic unit-cells, test specimens mounted in the large tube for: **d** sandwich acoustic structure and **e** composite sound absorber

Table 1 Structural parameters of the composite two acoustic unit-cell sound absorbers

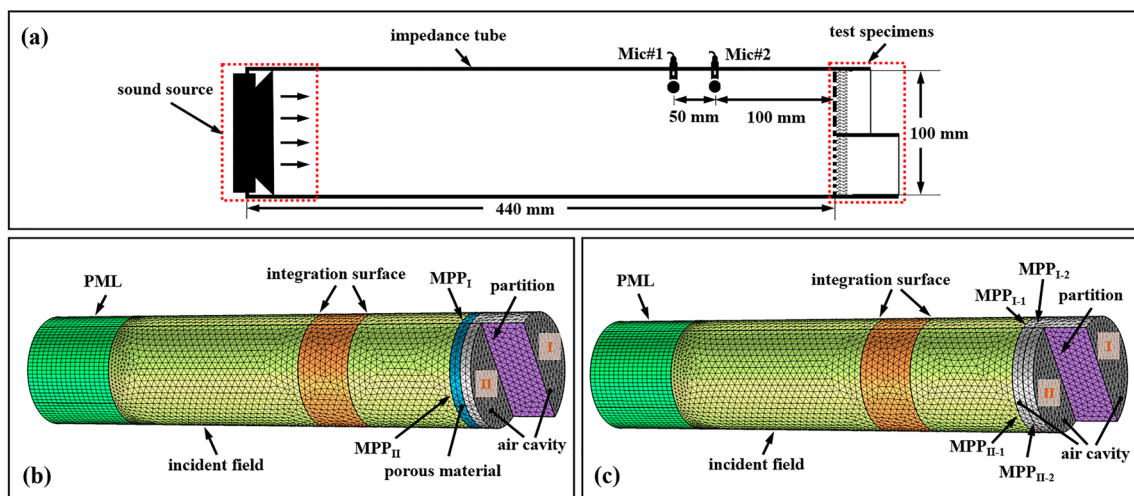
	depth of the air cavity layer (mm)				perforation ratio of the MPP layer (%)			
	D_{I-1}	D_{I-2}	D_{II-1}	D_{II-2}	p_{I-1}	p_{I-2}	p_{II-1}	p_{II-2}
Composite sound absorber	0	60	0	60	2	–	3	–
Sandwich acoustic structure	10	60	10	60	2	2	3	3

Table 2 Structural parameters of the composite three acoustic unit-cell sound absorbers

	Depth of the air cavity layer (mm)						Perforation ratio of the MPP layer (%)					
	D_{I-1}	D_{I-2}	D_{II-1}	D_{II-2}	D_{III-1}	D_{III-2}	p_{I-1}	p_{I-2}	p_{II-1}	p_{II-2}	p_{III-1}	p_{III-2}
Composite sound absorber	0	60	0	60	0	60	2	–	3	–	4	–
Sandwich acoustic structure	10	60	10	60	10	60	2	2	3	3	4	4

Table 3 Structural parameters of the composite four acoustic unit-cell sound absorbers

	Depth of the air cavity layer (mm)								Perforation ratio of the MPP layer (%)							
	D_{I-1}	D_{I-2}	D_{II-1}	D_{II-2}	D_{III-1}	D_{III-2}	D_{IV-1}	D_{IV-2}	p_{I-1}	p_{I-2}	p_{II-1}	p_{II-2}	p_{III-1}	p_{III-2}	p_{IV-1}	p_{IV-2}
Composite sound absorber	0	60	0	60	0	60	0	60	2	–	3	–	4	–	5	–
Sandwich acoustic structure	10	60	10	60	10	60	10	60	2	2	3	3	4	4	5	5

**Fig. 5** FE model of the impedance tube for the composite multi-cell sound absorber: **a** Schematic diagram of the impedance tube model, **b** the composite sound absorber and **c** the sandwich acoustic structure with two acoustic unit-cells

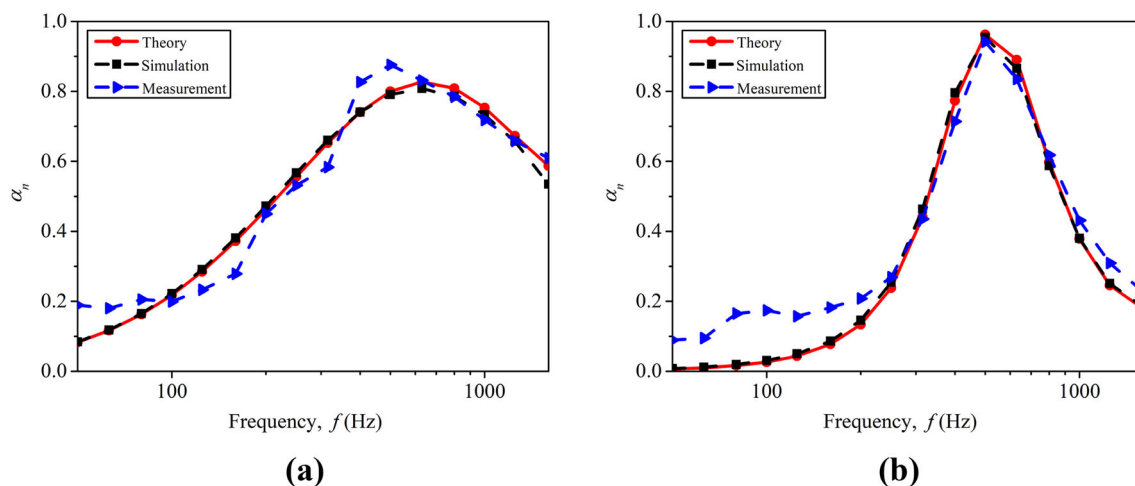


Fig. 6 Comparison of the measurement data, the theoretical value and the simulation results for: **a** composite sound absorber and **b** sandwich acoustic structure with two acoustic unit-cells

acoustic field and the composite multi-cell sound absorber. The external surfaces and the partitions of the impedance tube model were given the hard boundary condition, and the perfectly matched layer (PML) was used to model the impedance tube’s sound source end. The incident field and the air cavity layer were given the ambient air properties. The ambient air density was $\rho_0 = 1.225 \text{ kg/m}^3$, and the speed of the sound was $c_0 = 343 \text{ m/s}$. The MPP layers were defined with Maa’s model, and the Delany and Bazley’s model was selected for modelling the porous fibrous material layer. The integration surfaces were used for calculating the sound pressure at two different microphone positions so that the SAC of the composite multi-cell sound absorber could be calculated. It should be noted that a maximum element size of 5 mm was used to ensure the accuracy of the numerical analysis results.

5 Results and Discussion

5.1 Comparison of the Measurement Data and the Prediction Results

Figure 6 shows the comparison between the measurement data, the theoretical values and the simulation results for the composite two acoustic unit-cell sound absorber (where $p_{I-1} = 2\%$, $p_{II-1} = 3\%$, $D_{I-1} = D_{II-1} = 60 \text{ mm}$) and the sandwich acoustic structure (where $p_{I-1} = p_{I-2} = 2\%$, $p_{II-1} = p_{II-2} = 3\%$, $D_{I-1} = D_{II-1} = 10 \text{ mm}$, $D_{I-2} = D_{II-2} = 60 \text{ mm}$) as an example. In this paper, the theoretical values are calculated using Eqs. (1)–(16), and the theoretical results are very close to the simulation results, while the experimental values are deviated. Therefore, this paper introduces RMS (root-mean-square) error to describe this deviation. The RMS error between the measured sound absorption coefficient α_{mea} and

the predicted sound absorption coefficient α_{sim} over n frequencies can be calculated by [28]:

$$\text{RMS}_{\text{error}} = \sqrt{\frac{1}{n} \sum_{i=1}^n (\alpha_{\text{mea}} - \alpha_{\text{sim}})^2} \tag{17}$$

In this research, the RMS error for the composite of two acoustic unit-cell sound absorber and the sandwich acoustic structure is 6.27% and 8.18%, respectively. It should be noted that the RMS differences between the simulation results and the measurement data are less than 10% in the frequency range from 50 to 1600 Hz. The comparison results reveal that the experimental data have a reasonably good agreement with the simulation approach, which demonstrate that the simulation model based on the finite element model and impedance tube method is reliable. For the composite sound absorber, a higher peak SAC and a wider sound absorption bandwidth in the frequency range above 500 Hz were obtained. This is because the porous material has a good SAC at the higher frequencies. Moreover, there are some fluctuation peak values visible in the experiment results. These peaks usually correspond to the air resonance of the impedance tube and to the fundamental modes of the MPP layer itself. The impedance tube measurements are less accurate below 180 Hz because of the 50 mm microphone spacing.

5.2 Effect of the Structure Parameters

In general, the acoustic resonance frequency of the peak SAC and sound absorption bandwidth for a composite sound absorber can be controlled by the perforation ratio of the MPP layer and the depth of the air cavity layer [22]. In this paper, the effects of the perforation ratio of the different MPP layer and the depth of the air cavity layer on the SAC

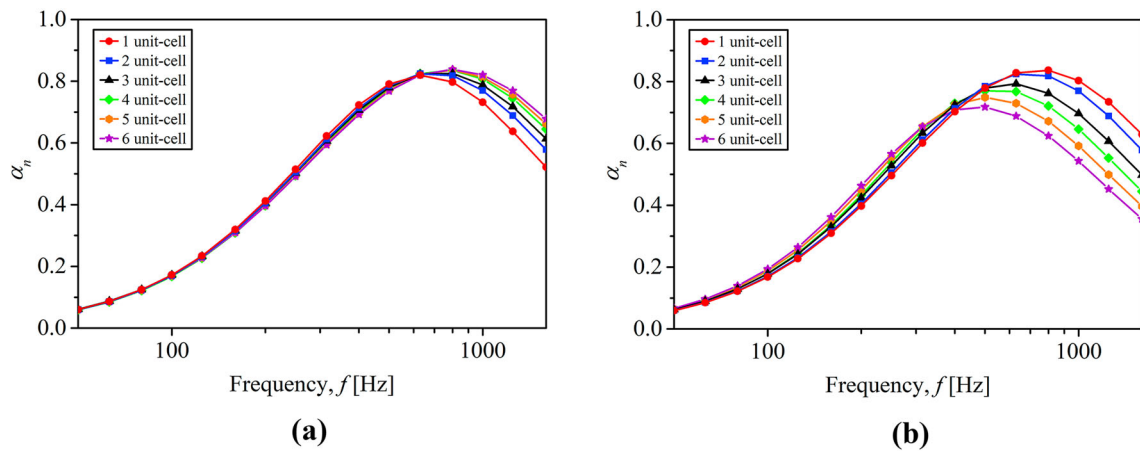


Fig. 7 The effect of the perforation ratio on the SACs for the composite sound absorber of: **a** the perforation ratio of the MPP layer increases with an increase of the number of the acoustic unit-cells and **b** the perforation ratio of the MPP layer decreases with an increase of the number of the acoustic unit-cells

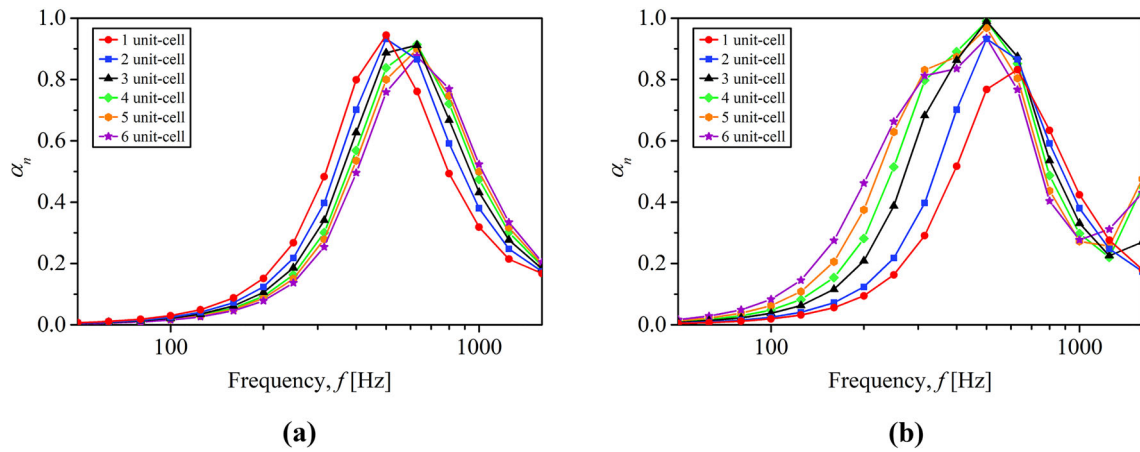


Fig. 8 The effect of the perforation ratio on the SACs for the sandwich acoustic structure of: **a** the perforation ratio of the MPP layer increases with an increase of the number of the acoustic unit-cells and **b** the perforation ratio of the MPP layer decreases with an increase of the number of the acoustic unit-cells

Table 4 Perforation ratio of the MPP layer of the composite sound absorber for the case corresponding to Fig. 7a

Number of the acoustic unit-cells	Perforation ratio of the MPP layer (%)					
	<i>pI-1</i>	<i>pII-1</i>	<i>pIII-1</i>	<i>pIV-1</i>	<i>pV-1</i>	<i>pVI-1</i>
1	2	–	–	–	–	–
2	2	3	–	–	–	–
3	2	3	4	–	–	–
4	2	3	4	5	–	–
5	2	3	4	5	6	–
6	2	3	4	5	6	7

Table 5 Perforation ratio of the MPP layer of the composite sound absorber for the case corresponding to Fig. 7b

Number of the acoustic unit-cells	Perforation ratio of the MPP layer (%)					
	p_{I-1}	p_{II-1}	p_{III-1}	p_{IV-1}	p_{V-1}	p_{VI-1}
1	3	–	–	–	–	–
2	3	2	–	–	–	–
3	3	2	1	–	–	–
4	3	2	1	0.8	–	–
5	3	2	1	0.8	0.6	–
6	3	2	1	0.8	0.6	0.4

Table 6 Perforation ratio of the MPP layer of the sandwich acoustic structure for the case corresponding to Fig. 8a

Number of the acoustic unit-cells	Perforation ratio of the MPP layer (%)											
	p_{I-1}	p_{I-2}	p_{II-1}	p_{II-2}	p_{III-1}	p_{III-2}	p_{IV-1}	p_{IV-2}	p_{V-1}	p_{V-2}	p_{VI-1}	p_{VI-2}
1	2	2	–	–	–	–	–	–	–	–	–	–
2	2	2	3	3	–	–	–	–	–	–	–	–
3	2	2	3	3	4	4	–	–	–	–	–	–
4	2	2	3	3	4	4	5	5	–	–	–	–
5	2	2	3	3	4	4	5	5	6	6	–	–
6	2	2	3	3	4	4	5	5	6	6	7	7

Table 7 Perforation ratio of the MPP layer of the sandwich acoustic structure for the case corresponding to Fig. 8b

Number of the acoustic unit-cells	Perforation ratio of the MPP layer (%)											
	p_{I-1}	p_{I-2}	p_{II-1}	p_{II-2}	p_{III-1}	p_{III-2}	p_{IV-1}	p_{IV-2}	p_{V-1}	p_{V-2}	p_{VI-1}	p_{VI-2}
1	3	3	–	–	–	–	–	–	–	–	–	–
2	3	3	2	2	–	–	–	–	–	–	–	–
3	3	3	2	2	1	1	–	–	–	–	–	–
4	3	3	2	2	1	1	0.8	0.8	–	–	–	–
5	3	3	2	2	1	1	0.8	0.8	0.6	0.6	–	–
6	3	3	2	2	1	1	0.8	0.8	0.6	0.6	0.4	0.4

of the composite multi-cell sound absorber are presented. Figure 7 and Fig. 8 show the effect of the perforation ratio on the SACs for the composite multi-cell sound absorber with two different conditions: one is the perforation ratio of the MPP layer increasing with an increase of the number of the acoustic unit-cells and the other is the perforation ratio of the MPP layer decreasing with an increase of the number of the acoustic unit-cells. It should be noted that the depth of the backed air cavity layer is 60 mm for each acoustic unit-cell, and the perforation ratio of the MPP layer of the composite sound absorber for the cases corresponding to Fig. 7a and b is shown in Tables 4 and 5, respectively. The results reveal that the SAC is improved when the perforation ratio of the MPP

layer increases with an increase of the number of the acoustic unit-cells in the frequency range from 800 to 1600 Hz. The SAC is gradually decreased when the perforation ratio of the MPP layer decreases with an increase of the number of the acoustic unit-cells in the frequency range from 400 to 1600 Hz. It should be noted that the SAC is very nearly simply a function of the mean value of the perforation ratio. For example, the SAC for three acoustic unit-cells with $p_{I-1} = 2$, $p_{II-1} = 3$ and $p_{III-1} = 4$ is indistinguishable from those for a single cell with $p_{I-1} = 3$. This results from Z_{MPP} being significantly larger than the combined impedance of the other elements, so that in this case Z_{s-i} in Eq. (15) is nearly equal to Z_{MPP-i} .

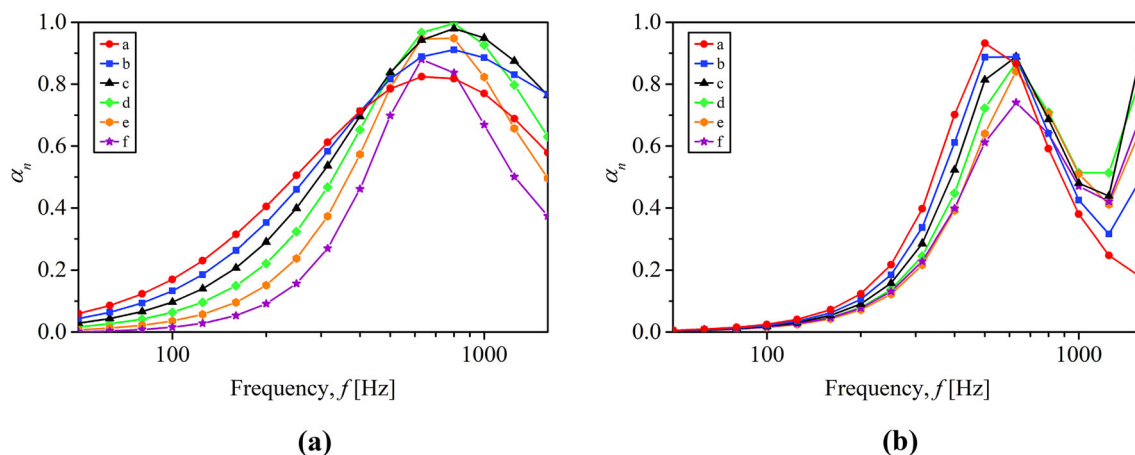


Fig. 9 The effect of the depth of the air cavity layer on the SACs of: **a** composite sound absorber and **b** sandwich acoustic structure with two acoustic unit-cells

Table 8 Structural parameters of the composite multi-cell sound absorbers for the case corresponding to Fig. 9

		Depth of the air cavity layer (mm)				Perforation ratio of the MPP layer (%)			
		D_{I-1}	D_{I-2}	D_{II-1}	D_{II-2}	p_{I-1}	p_{I-2}	p_{II-1}	p_{II-2}
Composite sound absorber	a	0	60	0	60	2	–	3	–
	b	10	50	10	50	2	–	3	–
	c	20	40	20	40	2	–	3	–
	d	30	30	30	30	2	–	3	–
	e	40	20	40	20	2	–	3	–
	f	50	10	50	10	2	–	3	–
Sandwich acoustic structure	a	10	60	10	60	2	2	3	3
	b	20	50	20	50	2	2	3	3
	c	30	40	30	40	2	2	3	3
	d	40	30	40	30	2	2	3	3
	e	50	20	50	20	2	2	3	3
	f	60	10	60	10	2	2	3	3

It should be noted that the perforation ratio of the MPP layer of the sandwich acoustic structure for the cases corresponding to Fig. 8a, b is shown in Tables 6 and 7, respectively. When the perforation ratio of the MPP layer increases with an increase of the number of the acoustic unit-cells, the peak of the SAC curve moved towards the high-frequency zone. However, as illustrated in Fig. 8b, when the perforation ratio of the MPP layer decreases with an increase of the number of the acoustic unit-cells, the sound absorption curve moved towards the low- and mid-frequency zones and the frequency bandwidth increased at the same time.

As illustrated in Fig. 9 and Table 8, the depth of the air cavity layer has a significant effect on the sound absorption coefficient for the composite multi-cell sound absorber. It should be noted that the total thickness of the air cavity

layer is kept at $D_I + D_{II} = 60$ mm for the composite sound absorber, and the results show that the sound absorption bandwidth continues to narrow by decreasing the depth of the air cavity layer D_I but increasing D_{II} . The peak SAC increases for the case of a, b, c, and d, but decreases for the case of e and f. For a sandwich acoustic structure, Fig. 9b shows that the depth of the air cavity layer D_I is increased but D_{II} is decreased, the total depth of the air cavity layer is kept at $D_I + D_{II} = 70$ mm, the sound absorption curve moves from low frequency to mid frequency, and the absorption resonance peak moves towards lower frequencies continuously. Therefore, the sound absorption bandwidth and the peak SAC can be effectively controlled by changing the thickness of the air cavity layer for the composite multi-cell sound absorber.

5.3 Optimization Results

In this paper, the GA was used to optimize the sound absorption coefficient of the composite multi-cell sound absorber. In this method, both constrained and unconstrained optimization problems can be solved based on natural selection, which is the process that drives biological evolution. In the GA, the objective function used for this study can be written as [40, 41]:

$$\max(A) = \int_{f_{\text{down}}}^{f_{\text{up}}} \alpha(f) df \quad (18)$$

where f_{up} and f_{down} denote the upper and lower limits of the frequency band of interest. In this paper, the frequency range is 50 Hz to 1600 Hz, and 10 Hz frequency steps are used to evaluate this integral.

The perforation ratio (mainly by adjusting the hole spacing) for the MPP layer and the depths of the air cavities are selected as the variable parameters. It should be noted that the depths of each air cavity layer were allowed to be varied and only the total thickness of the air cavities was constrained to 60 mm for the acoustic unit-cell of the composite sound absorber. For the sandwich acoustic structure, the total thickness of the air cavities was kept fixed at 70 mm and the depths of each air cavity layer were varied. Moreover, the range of the perforation ratio of the MPP layer is 0.5% to 5%, which is a reasonable range for these variable parameters based on the manufacturing process and the production conditions [37, 40]. In this paper, the GA toolbox of the MATLAB software was used to search for the optimized SAC results for the composite multi-cell sound absorber. The GA parameters were set as follows: PopSize = 100; MaxGeneration = 200; CrossProbability = 0.8 and VariationProbability = 0.01. It should be noted that the results converge reasonably well when using these parameters for the GA.

Figure 10 shows the comparison results of the unoptimized and optimized SAC curves of the composite multi-cell sound absorber with two acoustic unit-cells, three acoustic unit-cells, and four acoustic unit-cells. The optimized variable parameters for the composite sound absorber and sandwich acoustic structure which correspond to the cases in Fig. 10 are listed in Tables 9, 10 and 11, respectively. The results revealed that the SAC of the composite multi-cell sound absorbers has significantly improved for both the composite sound absorber and the sandwich acoustic structure. The acoustic resonance frequency of the peak SAC of the optimized composite sound absorber becomes higher but decreases of the absorption bandwidth. The sound absorption bandwidth of the optimized sandwich acoustic structure is significantly broadened as shown in Fig. 10b, d, f. Moreover, it should be noted that the optimized perforation ratio of the MPP in 2, 3, and 4 unit-cells for the composite sound absorber appeared many times

to take the maximum value of 5%. It was also shown that for composite sound absorber increasing the perforation ratio of the MPP helps to improve the sound absorption performance in the mid-frequency band (400–1600 Hz). However, for the sandwich acoustic structure, the optimization results reveal that each optimized perforation ratio of the MPP layer increases the minimum value of the perforation ratio by 0.5%, which shows that the sound absorption bandwidth is widened effectively with the decrease of the perforation ratio of the MPP layer.

The perforation ratios of the outer MPP layer of the composite multi-cell sound absorber were close to the maximum value. Nevertheless, for the sandwich acoustic structure, the perforation ratio of the outer MPP layer was always greater than that of the inner MPP layer. The results show that increasing the perforation ratio of the outer MPP layer is beneficial for the improvement of the acoustic performance of the composite multi-cell sound absorber. Figure 11 shows the comparison of the theoretical values and the FE simulation results for the optimized composite multi-cell sound absorbers with two acoustic unit-cells. The theoretical values are in good agreement with the finite element simulation results. Since the FE simulation model of the impedance tube established in this paper is considered to be fairly accurate, it verifies the performance of the optimized composite multi-cell sound absorbers.

Table 12 shows the average SAC of the unoptimized and optimized composite multi-cell sound absorber in the frequency range from 400 to 1600 Hz. The optimized composite multi-cell sound absorbers have significantly improved average sound absorption coefficients, and they have wider sound absorption bandwidths in their frequency range. The average sound absorption coefficient of the optimized composite sound absorber with 2, 3, and 4 acoustic unit-cells has been improved by 18.9%, 18.2%, 17.3%. The average sound absorption coefficient of the optimized sandwich acoustic structure with 2, 3, and 4 acoustic unit-cells has been improved by 92.6%, 80.2%, 78.4%, respectively. Hence, the acoustic properties of the composite multi-cell sound absorber can be significantly improved by tuning the various depths of the air cavities and the perforation ratios of the MPP layers when the total thickness is constrained. In addition, the composite sound absorber has better sound absorption performance than the sandwich acoustic structure before the optimization and its structure is much simpler. However, the sound absorption performance of the sandwich acoustic structure is greatly improved by using the GA, especially at low and middle frequencies. It is suitable for the case where more emphasis is placed on low- and middle-frequency sound absorption and where porous materials cannot be used in practical applications.

Figure 12 shows the comparison of the SAC results for the unoptimized and the optimized composite multi-cell sound

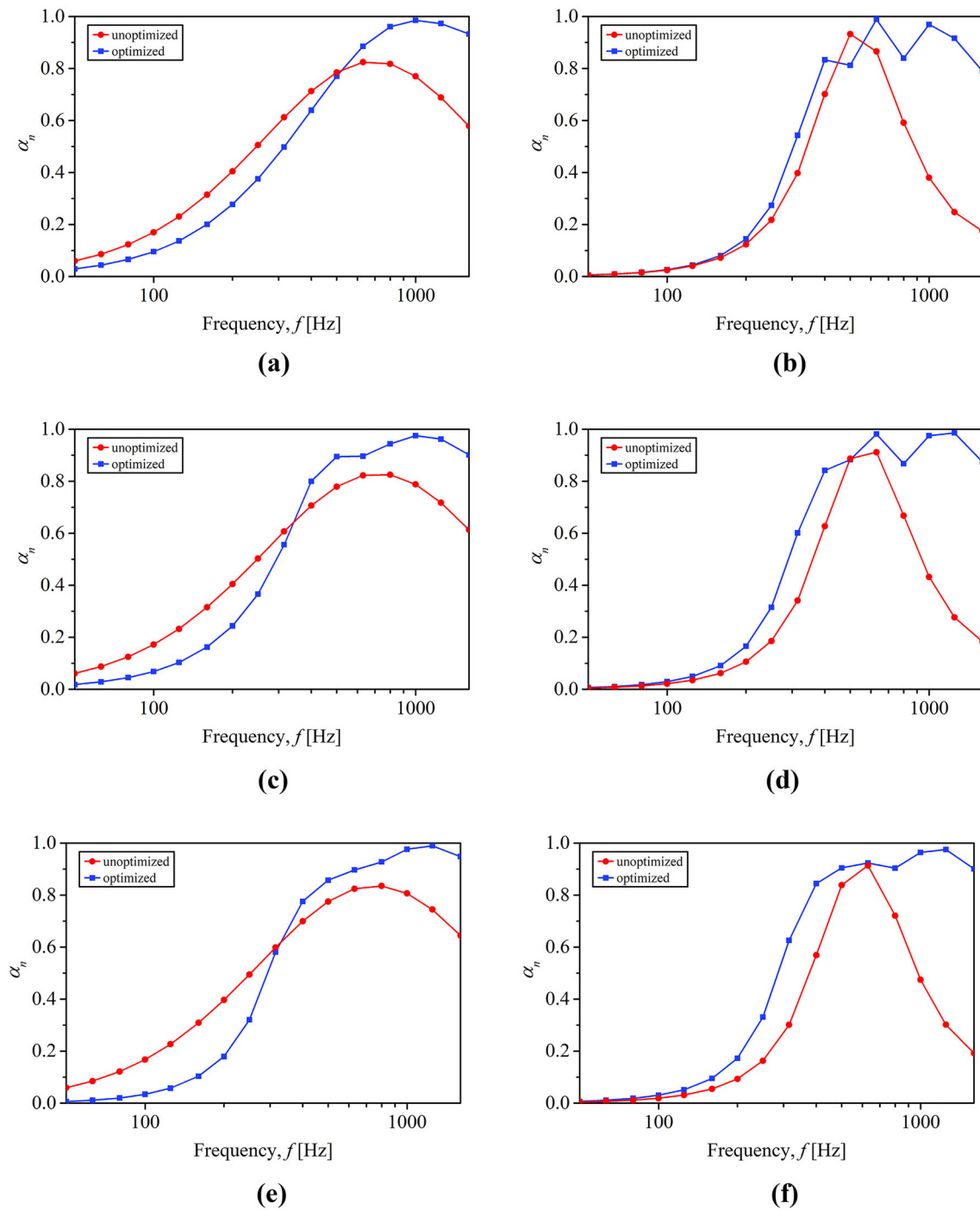


Fig. 10 Comparison of the SACs of the original and optimized for the composite multi-cell sound absorber: composite sound absorber with **a** two acoustic unit-cells, **c** three acoustic unit-cells and **e** four acoustic unit-cells, respectively; sandwich acoustic structure with **b** two acoustic unit-cells, **d** three acoustic unit-cells and **f** four acoustic unit-cells, respectively

Table 9 Optimized variable parameters for the composite multi-cell sound absorber with two acoustic unit-cells

	Depth of the air cavity layer (mm)				Perforation ratio of the MPP layer (%)			
	D_{I-1}	D_{I-2}	D_{II-1}	D_{II-2}	p_{I-1}	p_{I-2}	p_{II-1}	p_{II-2}
Composite sound absorber	21.3	38.7	17.0	43.0	5	–	2.75	–
Sandwich acoustic structure	34.2	35.8	40.2	29.8	1.77	0.5	4.58	1.23

Table 10 Optimized variable parameters for the composite multi-cell sound absorber with three acoustic unit-cells

	Depth of the air cavity layer (mm)						Perforation ratio of the MPP layer (%)					
	D_{I-1}	D_{I-2}	D_{II-1}	D_{II-2}	D_{III-1}	D_{III-2}	p_{I-1}	p_{I-2}	p_{II-1}	p_{II-2}	p_{III-1}	p_{III-2}
Composite sound absorber	25.1	34.9	24.8	35.2	42.0	18.0	5	–	5	–	0.93	–
Sandwich acoustic structure	23.6	44.4	43.3	26.7	40.8	29.2	1.95	0.5	2.05	0.5	5	1.4

Table 11 Optimized variable parameters for the composite multi-cell sound absorber with four acoustic unit-cells

	Depth of the air cavity layer (mm)								Perforation ratio of the MPP layer (%)							
	D_{I-1}	D_{I-2}	D_{II-1}	D_{II-2}	D_{III-1}	D_{III-2}	D_{IV-1}	D_{IV-2}	p_{I-1}	p_{I-2}	p_{II-1}	p_{II-2}	p_{III-1}	p_{III-2}	p_{IV-1}	p_{IV-2}
Composite sound absorber	38.2	21.8	56.4	3.6	42.5	17.5	43.5	16.5	5	–	0.63	–	5	–	1.44	–
Sandwich acoustic structure	21.4	48.6	48.5	21.5	31.4	38.6	42.7	23.7	2.3	0.5	2.4	0.5	2.30	0.5	5	1.71

Table 12 The average SAC of the unoptimized and optimized composite multi-cell sound absorber in the frequency range from 400 to 1600 Hz

	Average SAC		
	Two acoustic unit-cell	Three acoustic unit-cell	Four acoustic unit-cell
Composite sound absorber	0.736	0.752	0.768
Sandwich acoustic structure	0.475	0.521	0.528
Optimized composite sound absorber	0.925	0.934	0.941
Optimized sandwich acoustic structure	0.915	0.940	0.942

absorbers with two acoustic unit-cells where the optimization has been carried out in the frequency range from 50 to 400 Hz and in the frequency range from 50 to 1600 Hz, respectively. The improvement in the sound absorption coefficients shown in Fig. 10 is largely in the frequency range from 400 to 1600 Hz, and in fact the optimized design sometimes gives lower SACs in the frequency range from 50 to 400 Hz. The increase in sound absorption can be moved to lower frequencies by changing the objective function, Eq. (18), to cover only the low frequency range. For the composite sound absorber with two acoustic unit-cells, the optimization at low frequencies is limited by structural parameters.

6 Conclusions

In this paper, the sound absorption coefficients of a composite multi-cell sound absorber were calculated. The theoretical predictions were made using the transfer matrix method and with the equivalent circuit method for the composite multi-cell sound absorber. A finite element numerical model of an impedance tube was used to validate the sound absorption

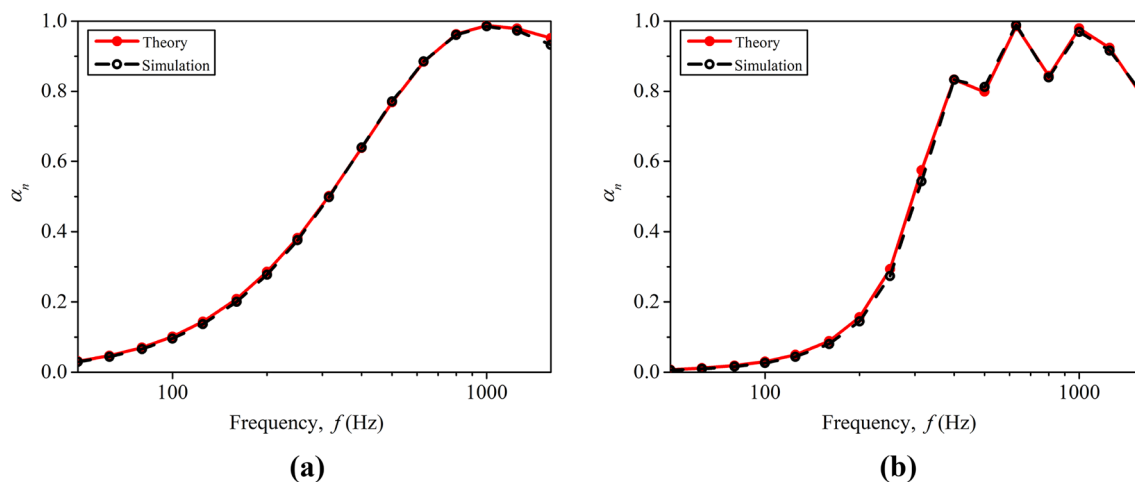


Fig. 11 Comparison of the theoretical values and the FE simulation results for: **a** the optimized composite sound absorber and **b** the optimized sandwich acoustic structure with two acoustic unit-cells

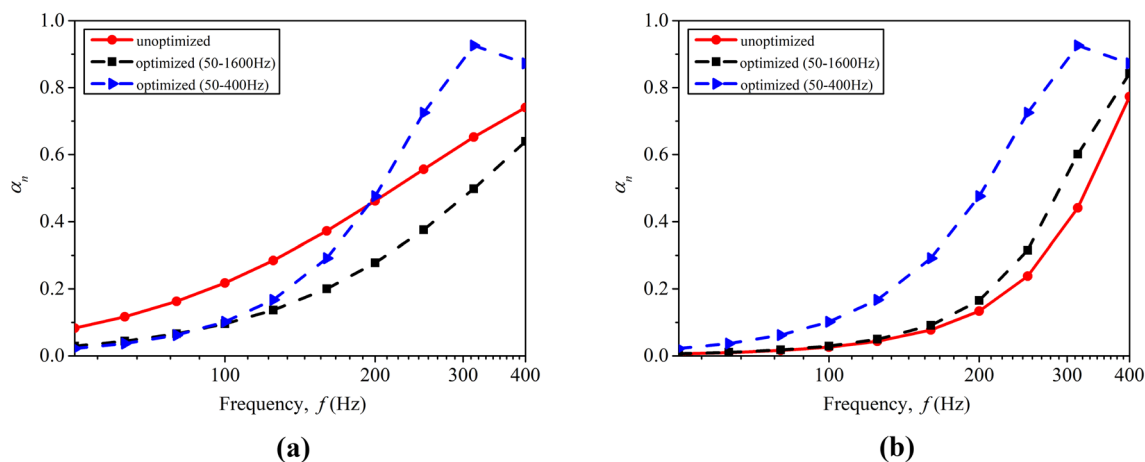


Fig. 12 Comparison of the SACs optimized in 50–400 Hz range and optimized in 50–1600 Hz range for the composite multicell sound absorber: **a** composite sound absorber and **b** sandwich acoustic structure with two acoustic unit-cells

coefficients measured using the two-microphone impedance tube method. The comparison of the results showed that the theoretical approach has a reasonably good agreement with the measurement data. The effect of the structure parameters, such as the perforation ratio and the thickness of the air cavity layer, was investigated. The results indicated that changes in the perforation ratio of the different MPP layers and the depth of the air cavity layer of the composite multi-cell sound absorber led to a shift in frequency and change in the value of the resonant peak sound absorption coefficient. Increasing the number of the acoustic unit-cells improved the sound absorption performance of the composite sound absorber. The results showed that a composite sound absorber optimized using the genetic algorithm can generate a broader sound absorption bandwidth and higher average sound absorption coefficient. The significant improvement of the sound absorption coefficient in the middle-frequency range from 600 to 1600 Hz confirmed that optimizing the

sound absorption coefficients of composite multi-cell structures using the GA is effective. The results presented in this paper are beneficial for enhancing acoustic design and refining acoustic quality.

Acknowledgements This research was supported by Zhejiang Provincial Natural Science Foundation of China under Grant No. LQ20E050022. The authors would like to thank Zhejiang Jiuzhou New Energy Technology Co., Ltd. and RMIT's Advanced Manufacturing Precinct (AMP, Melbourne, Australia) for providing a series of test samples and technical help. The scholarship provided to Yujun Zhao by RMIT University is gratefully acknowledged. The assistance of Jinhui Xu from the School of Engineering, RMIT University, in preparing a series of experimental setups is gratefully acknowledged.

References

1. Tang, X., Yan, X.: Acoustic energy absorption properties of fibrous materials: a review. *Compos. A Appl. Sci. Manuf.* **101**, 360–380 (2017)

2. Asdrubali, F., Schiavoni, S., Horoshenkov, K.V.: A review of sustainable materials for acoustic applications. *Build. Acoust.* **19**(4), 283–312 (2012)
3. Bravo, T., Maury, C., Pinhèdeb, C.: Optimising the absorption and transmission properties of aircraft microperforated panels. *Appl. Acoust.* **79**, 47–57 (2014)
4. Wang, Y., Zhu, X., Zhang, T., Wang, Y.: A renewable low-frequency acoustic energy harvesting noise barrier for high-speed railways using a Helmholtz resonator and a PVDF film. *Appl. Energy* **230**, 52–61 (2018)
5. Liu, Z.Q., Fard, M., Davy, J.L.: Prediction of the acoustic effect of an interior trim porous material inside a rigid-walled car air cavity model. *Appl. Acoust.* **165**, 107325 (2020)
6. Taban, E., Soltani, P., Berardi, U.: Measurement, modeling, and optimization of sound absorption performance of Kenaf fibers for building applications. *Build. Environ.* **180**, 107087 (2020)
7. Maa, D.Y.: Practical single MPP absorber. *Int. J. Acoust. Vibr.* **1**(12), 3–6 (2007)
8. Liu, J., Herrin, D.W.: Enhancing micro-perforated panel attenuation by partitioning the adjoining cavity. *Appl. Acoust.* **71**(2), 120–127 (2010)
9. Meng, H., Ao, Q.B., Ren, S.W.: Anisotropic acoustical properties of sintered fibrous metals. *Compos. Sci. Technol.* **107**(11), 10–17 (2015)
10. Dupont, T., Leclaire, P., Sicot, O., Gong, X.L., Panneton, R.: Acoustic properties of air-saturated porous materials containing dead-end porosity. *J. Appl. Phys.* **110**(9), 94903 (2011)
11. Liu, C.R., Wu, J.H., Yang, Z.: Ultra-broadband acoustic absorption of a thin microperforated panel metamaterial with multi-order resonance. *Compos. Struct.* **246**, 112366 (2020)
12. Zhao, X., Fan, X.: Enhancing low frequency sound absorption of micro-perforated panel absorbers by using mechanical impedance plates. *Appl. Acoust.* **88**, 123–128 (2015)
13. Qian, Y.J., Kong, D.Y., Liu, Y.: Improvement of sound absorption characteristics under low frequency for micro-perforated panel absorbers using super-aligned carbon nanotube arrays. *Appl. Acoust.* **82**, 23–27 (2014)
14. Ning, J.F., Ren, S.W., Zhao, G.P.: Acoustic properties of micro-perforated panel absorber having arbitrary cross-sectional perforations. *Appl. Acoust.* **111**, 135–142 (2016)
15. Maa, D.Y.: Microperforated-panel wideband absorber. *Noise Control Eng. J.* **29**(3), 77–84 (1987)
16. Zhang, Z.M., Gu, X.T.: The theoretical and application study on a double layer microperforated sound absorption structure. *J. Sound Vib.* **215**(3), 399–405 (1998)
17. Sakagami, K., Morimoto, M., Koike, W.: A numerical study of double-leaf microperforated panel absorbers. *Appl. Acoust.* **67**(7), 609–619 (2006)
18. Kim, H.S., Kim, S.R., Kim, B.K.: Sound transmission loss of multi-layered infinite micro-perforated plates. *J. Acoust. Soc. Am.* **147**(1), 508–515 (2020)
19. Kim, H.S., Ma, P.S., Kim, B.K., Lee, S.H., Seo, Y.H.: Sound transmission loss of multi-layered elastic micro-perforated plates in an impedance tube. *Appl. Acoust.* **166**, 107348 (2020)
20. Park, S.H.: Acoustic properties of micro-perforated panel absorbers backed by Helmholtz resonators for the improvement of low-frequency sound absorption. *J. Sound Vib.* **332**, 4895–4911 (2013)
21. Wang, C.Q., Cheng, L., Pan, J.: Sound absorption of a micro-perforated panel backed by an irregular-shaped cavity. *J. Acoust. Soc. Am.* **127**(1), 238–246 (2010)
22. Liu, Z.Q., Zhan, J.X., Fard, M., Davy, J.L.: Acoustic properties of multilayer sound absorbers with a 3D printed micro-perforated panel. *Appl. Acoust.* **121**, 25–32 (2017)
23. Yilmazer, S., Ozdeniz, M.B.: The effect of moisture content on sound absorption of expanded perlite plates. *Build. Environ.* **40**(3), 311–318 (2005)
24. Sakagami, K., Nagayama, Y., Morimoto, M., Yairi, M.: Pilot study on wideband sound absorber obtained by combination of two different microperforated panel (MPP) absorbers. *Acoust. Sci. Technol.* **30**, 154–156 (2009)
25. Gai, X.L., Xing, T., Li, X.H.: Sound absorption of microperforated panel with L shape division cavity structure. *Appl. Acoust.* **122**, 41–50 (2017)
26. Kim, H.S., Ma, P.S., Kim, B.K.: Low-frequency sound absorption of elastic micro-perforated plates in a parallel arrangement. *J. Sound Vib.* **460**, 114884 (2019)
27. Li, X., Wu, Q., Kang, L.: Design of multiple parallel-arranged perforated panel absorbers for low frequency sound absorption. *Materials* **12**(13), 2099 (2019)
28. Midori, K., Kimihiro, S., Takeshi, O.: A basic study on the absorption properties and their prediction of heterogeneous micro-perforated panels: a case study of micro-perforated panels with heterogeneous hole size and perforation ratio. *Acoustics* **3**, 473–484 (2021)
29. Zhao, H., Wang, Y., Yu, D., Yang, H., Zhong, J., Wu, F., Wen, J.: A double porosity material for low frequency sound absorption. *Compos. Struct.* **239**, 111978 (2020)
30. Rafique, F., Wu, J.H., Naqvi, S.M.A.: Enhanced wideband low-frequency sound absorption of a single-layer multiple parallel-arranged inhomogeneous microperforated panel absorber. *Acoust. Australia* **50**, 49–69 (2022)
31. Delany, M., Bazley, E.: Acoustical properties of fibrous absorbent materials. *Appl. Acoust.* **3**(2), 105–116 (1970)
32. Song, B.H., Bolton, J.S.: A transfer-matrix approach for estimating the characteristic impedance and wave numbers of limp and rigid porous materials. *J. Acoust. Soc. Am.* **107**(3), 1131–1152 (2000)
33. Lee, D.H., Kwon, Y.P.: Estimation of the absorption performance of multiple layer perforated panel system by transfer matrix method. *J. Sound Vib.* **278**(4–5), 847–860 (2004)
34. Zhu, C., Huang, Q.: A method for calculating the absorption coefficient of a multi-layer absorbent using the electro-acoustic analogy. *Appl. Acoust.* **66**, 879–887 (2005)
35. Pieren, R., Heutschi, K.: Predicting sound absorption coefficients of lightweight multilayer curtains using the equivalent circuit method. *Appl. Acoust.* **92**, 27–41 (2015)
36. Maa, D.Y.: Theory and design of microperforated panel sound-absorbing construction. *Sci. China* **18**, 55–71 (1975)
37. Maa, D.Y.: Potential of microperforated panel absorber. *J. Acoust. Soc. Am.* **104**(5), 2861–2866 (1998)
38. ASTM, ASTM C522-03: Standard test method for airflow resistance of acoustical materials, ASTM International, West Conshohocken, PA (2003).
39. ASTM, ASTM E1050-12: Standard test method for impedance and absorption of acoustical materials using a tube, two microphones and a digital frequency analysis system, ASTM International, West Conshohocken, PA (2012).
40. Zhao, X.D., Zhang, X.J., Jiang, Z.: Three layer microperforated panel optimal design and analysis of its characteristic. *Acta Acustica* **33**(1), 84–87 (2008)
41. Holland, J.H.: Outline for a logical theory of adaptive systems. *J. Assoc.* **9**(3), 297–314 (1962)

Publisher's Note Springer Nature remains neutral with regard to jurisdictional claims in published maps and institutional affiliations.

Springer Nature or its licensor (e.g. a society or other partner) holds exclusive rights to this article under a publishing agreement with the author(s) or other rightsholder(s); author self-archiving of the accepted manuscript version of this article is solely governed by the terms of such publishing agreement and applicable law.